Optical Control in Coupled Two-Electron Quantum Dots

L. Sælen,[1] R. Nepstad,[1] I. Degani,[2] and J. P. Hansen[1]
[1]Department of Physics and Technology, University of Bergen, N-5007 Bergen, Norway
[2]Department of Mathematics, University of Bergen, 5008 Bergen, Norway
(Received 14 August 2007; published 1 February 2008)

The dynamics of two electrons in a 2-dimensional quantum dot molecule in the presence of a time-dependent electromagnetic field is calculated from first principles. We show that carefully selected microwave pulses can exclusively populate a single state of the first excitation band and that the transition time can be further decreased by optimal pulse control. Finally we demonstrate that an oscillating charge localized state may be created by multiple transitions using a sequence of pulses.

DOI: 10.1103/PhysRevLett.100.046805 PACS numbers: 73.21.La, 78.20.Bh, 78.67.−n, 85.35.Be

Coherent control of interacting electrons in quantum dot molecules exposed to pulsed electromagnetic radiation is of fundamental interest and importance for a wide range of applications, from charge transport devices to quantum information [1–5]. In quantum information theory optical manipulation is an alternative to storing qubits in the electron spin [6,7], and an ''all optical quantum gate'' based on four low-lying two-electron states was recently experimentally verified with around 65% fidelity [8]. The short transition time in optically driven processes reduces the effect of decoherence sources, such as hyperfine [4] or phonon interactions [9]. However, effective utilization of transitions between excited states requires precise knowledge of the energy spectrum defined by the confining potential and the electron-electron interaction. Theoretical models accompanied by accurate calculations in this context demonstrate the true and ideal time development of the system and thus allow for assessment of possible realistic control schemes.

Theory of charge transport and excitation in one- and two-electron dots is most often based on restricted Hilbert space models, simplified Hubbard-like models, or continuum approaches [10–12]. In the present Letter we demonstrate, based on precise quantum simulations, optically driven transitions using picosecond pulses between excited states of a double quantum dot molecule with near 100% fidelity. The evolution of the system is obtained by solving the time-dependent two-electron Schrödinger equation numerically without any further approximations. Coherent two-electron charge transport is demonstrated, and we successfully apply a control algorithm to further optimize transition times and fidelity. To the best of our knowledge neither optical control nor optimization have previously been achieved in a two-electron double quantum dot.

The Hamiltonian of two interacting electrons in a double quantum dot with interdot distance d is modeled as a two-dimensional double harmonic oscillator [13,14],

$$\hat{H} = h(\mathbf{r}_1) + h(\mathbf{r}_2) + \frac{e^2}{4\pi\epsilon_r\epsilon_0 r_{12}}, \tag{1}$$

where

$$h(x,y) = -\frac{\hbar^2}{2m^*}\nabla^2 + \frac{1}{2}m^*\omega^2\left[\left(|x| - \frac{d}{2}\right)^2 + y^2\right] + V_{\text{ext}}(\mathbf{r},t). \tag{2}$$

Furthermore, $\mathbf{r}_{1,2}$ are single-particle coordinates and $r_{12} = |\mathbf{r}_1 - \mathbf{r}_2|$. The material parameters are taken as those of GaAs, with effective mass $m^* = 0.067m_e$ and relative permittivity $\epsilon_r = 12.4$. The confinement strength is here taken to be a typical ''experimental'' value, $\hbar\omega = 1$ meV [4]. The interaction with an external electromagnetic field, linearly polarized along the interdot direction, is expressed within the dipole approximation as

$$V_{\text{ext}}(\mathbf{r}_i, t) = Ef(t)\cos(\omega t)x_i, \tag{3}$$

where $i = 1, 2$, E is the field strength, $f(t)$ is the pulse envelope, and ω is the central frequency. The Hamiltonian is spin-conserving and the exact wave function at any time, $\Psi(t)$, may be obtained from an expansion in symmetrized basis states of one-center single-particle harmonic oscillator eigenfunctions ϕ_i,

$$\Psi = \sum_{j\geq i}^{n_{\max}} c_{ij}(t)\begin{cases}\frac{1}{\sqrt{2}}[\phi_i(\mathbf{r}_1)\phi_j(\mathbf{r}_2) + \phi_j(\mathbf{r}_1)\phi_i(\mathbf{r}_2)] & i \neq j,\\ \phi_i(\mathbf{r}_1)\phi_j(\mathbf{r}_2) & i = j,\end{cases} \tag{4}$$

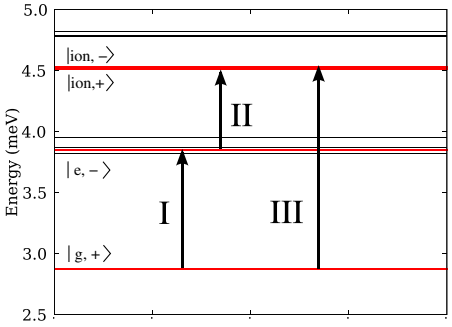

FIG. 1 (color online). The figure shows the 10 lowest singlet energy levels of the field free Hamiltonian of Eq. (1) with $d = 130$ nm, $V_{\text{ext}} = 0$, and $\hbar\omega = 1$ meV. The $\pm$ indicates the x parity of the highlighted states.

with $i, j = \{n_x, n_y\}$ representing the quantum numbers of the Hermite polynomials in x and y, respectively. The spectrum of the field free Hamiltonian was recently classified as a function of the interdot distance d [15]. The lower part of the resulting singlet spectrum for $d = 130$ nm is shown in Fig. 1. We observe a clustering of levels into energy bands which can be understood and fairly accurately described by the behavior at asymptotically large interdot distances: The ground state, $|g, ++\rangle$, has positive parity in both the x and the y direction (indicated, respectively) and is essentially a combination of the ground states of two harmonic oscillators centered at $\pm d/2$. The second band has four excited states which contain a single excited quanta (n_x^L, n_y^L, n_x^R, or $n_y^R = 1$) and are of the form,

$$\phi_{10}(\mathbf{r}_{1L})\phi_{00}(\mathbf{r}_{2R}) + \phi_{00}(\mathbf{r}_{1L})\phi_{10}(\mathbf{r}_{2R}) + \phi_{10}(\mathbf{r}_{1R})\phi_{00}(\mathbf{r}_{2L}) + \phi_{00}(\mathbf{r}_{1R})\phi_{10}(\mathbf{r}_{2L}), \tag{5}$$

with the L, R subscripts denoting left and right centered orbitals, respectively. The four singly excited states can be classified with respect to positive or negative parity as $\{|e_1, --\rangle, |e_2, -+\rangle, |e_3, +-\rangle, |e_4, ++\rangle\}$. The third energy band contains two excited states of different x parity, $\{|\text{ion}_5, ++\rangle, |\text{ion}_6, -+\rangle\}$, which asymptotically correlate to the two-electron ground state of a single dot, in analogy with ionic states of diatomic molecules. The states can be inspected by plotting the single-particle electron density, $\rho(r) = \int d^2 r_2 |\Psi(r, r_2)|^2$, shown in Fig. 2 for the states $|g, ++\rangle$, $|e_2, -+\rangle$, and $|\text{ion}_6, -+\rangle$. Shown in Fig. 2 are also the conditional single-electron densities obtained by fixing all degrees of freedom except one x component at a maximum of the wave function, and similarly for the other x component (electron). The densities of the ground state $|g, +\rangle$ and the second excited state $|e, -\rangle$ (upper and middle panels) are seen to have the characteristics of two displaced eigenstates of the harmonic oscillator, and the conditional densities clearly show that "one" electron is centered in each dot. Note that we have suppressed the y parity and state number to simplify notation. The state $|\text{ion}, -\rangle$ (lower panel), in contrast, shows a high probability that both electrons occupy the same dot. As mentioned, in a basis of asymptotic states the two ionic states $|\text{ion}, \pm\rangle$ resemble the entangled states

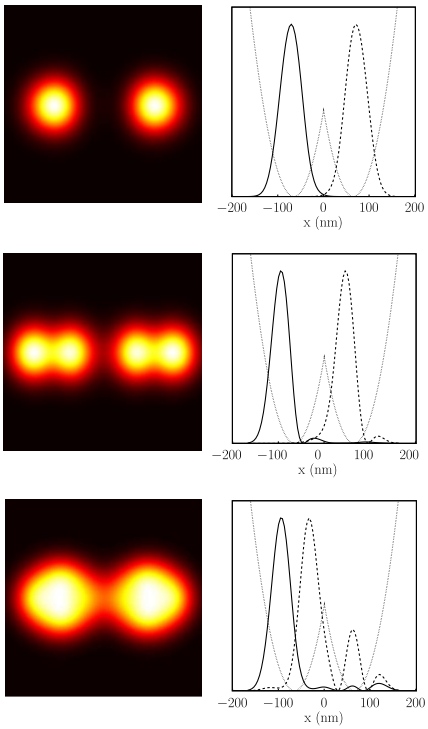

FIG. 2 (color online). One-electron densities (left column) and conditional densities (right column). The conditional densities are evaluated at one maximum of the wave function, for each electron (solid and dashed lines). Upper panel: ground state, middle panel: 2nd excited state, and lower panel: 6th excited state. The right column shows that the two upper states may be regarded as "covalent" states, whereas the lower state is an "ionic" state with both electrons in the same dot. The double dot potential is also shown. The interdot distance is $d = 130$ nm. Both axes in the left column range from −165 to 165 nm.

$$|g(r_{1L}, r_{2L})\rangle \pm |g(r_{1R}, r_{2R})\rangle, \tag{6}$$

where $|g\rangle$ refers to the shifted ground state of a single two-electron dot.

On this background we may construct optically controlled transitions: With an x-polarized field direct transitions from a state $|i\rangle$ to another state $|f\rangle$ occur only between states of opposite x parity, and thus a one-photon transition from the ground state is allowed only to the $|e, -\rangle$ and $|\text{ion}, -\rangle$ states, as indicated in Fig. 1. We now explore whether such transitions can be obtained with unit probability at intensities high enough to secure fast transitions, but without exciting nonresonant transitions. Furthermore, we seek a complete transition from the ground state to a configuration where both electrons occupy either the left or right dot, using a combination of different pulses. The dynamics will be governed by the time evolution of the coefficients of Eq. (4), $\dot{c}_{ij}(t) = -i\sum_{i'j'} c_{i'j'}(t)\langle i'j'|\hat{H}|ij\rangle$. The dynamics calculations with $n_{y,\max} = 4$ and $n_{x,\max} = 14$ were thoroughly checked for convergence. The theoretical analysis and demonstration below based on the harmonic potential is in the present context restrictive since anharmonicity in general will yield a less regular energy spacing [16]. This would lower the probability for "unwanted" excitations higher up in the spectrum, and thus act as a restoring force for quantum control [17].

The upper panel of Fig. 3 displays the population transfer from the initial $|g, +\rangle$ state and the $|e, -\rangle$ state for a pulse of the form of Eq. (3). The frequency is tuned to the energy difference of the two states, $\omega_I = 1.5$ THz. The envelope function is $f_I = \sin^2(\frac{\pi}{T_I} t)$. A complete two-level-

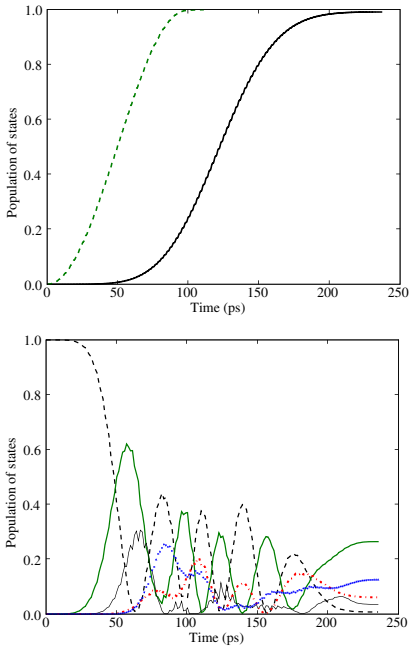

FIG. 3 (color online). Upper panel: Controlled transition from the ground state to the first excited state, $|g, +\rangle \rightarrow |e, -\rangle$ with $\omega_I = 1.5$ THz and $I_I = 0.39$ W/cm^2 (solid line). The dashed curve shows the transition using an optimized pulse. Lower panel: Time development of a few selected states for the same pulse as above with intensity $I_I = 3.86$ W/cm^2. The population shown is for the ground state (thick dashed line), second excited state (thick solid line), 7th excited state (dash-dotted line), 11th excited state (thin solid line), and 24th excited state (dotted line).

like transition is achieved with interaction time $T_I = 237$ ps (15 cycles).

The pulse applied above is rather simple, using a single frequency and a standard envelope function. More complex, nonintuitive pulses that are specifically designed for a certain target state might have better performance in terms of higher fidelity and shorter transition times. For the purpose of obtaining such tailored pulses, optimal control theory has had great theoretical success in recent years [18,19]. To explore the usefulness of control theory in the present context, we have applied Krotov's algorithm [18] to optimize the transition to the first excitation band. The algorithm aims to maximize $|\langle\Psi(T)|e, -\rangle|^2$ while minimizing the laser energy. The result of the calculation is given in Fig. 3, showing complete transition within half the original transition time. Speedups of 2–10 times that of conventional pulse durations needed for complete transitions were recently demonstrated for one-electron quantum dot systems [20,21]. In the present Letter we focus on physical mechanisms and simple pulses. However, even faster transitions may be achievable with more sophisticated polarization optimized pulses [22].

The lower panel of Fig. 3 displays the sensitivity to field intensity in the present system, showing a few of the most prominent components of the wave function during the pulse. Increasing the pulse amplitude by a factor of 10 connects nearly all states, and we obtain an irregular time development with significant projection on a large number of states. The system becomes highly excited and only $\approx$54% of the wave function is represented by the 50 lowest states. The high intensity of the field causes a broadening of the absorption lines (saturation), and the transition probability for even far off-resonant states may become sizable. Indeed an estimate of the width at half maximum of the resonance corresponding to a single photon resonance, $\Gamma \simeq 2E\langle i|x_1 + x_2|j\rangle$ [23], reveals non-negligible probabilities for nearly all allowed transitions in the spectrum. In this case the dynamics is composed of many individual step transitions originating from the ground state and cannot be accurately described within simple models.

Proceeding to charge transport we observe that, from the analysis of the spectrum in Fig. 2, a charge localized state can be realized by an equal linear combination of the two ionic states, $|\text{ion}, \pm\rangle$,

$$|\Psi_{\text{CLS}}\rangle = \frac{1}{\sqrt{2}}(e^{-iE_+ t}|\text{ion}, +\rangle + e^{-i(E_- t+\gamma)}|\text{ion}, -\rangle), \quad (8)$$

where γ is an arbitrary phase difference. The two electrons will oscillate between being localized in the left and the right dot, with a period of 180 ps given by the energy difference of the two ionic states. Based on the ability to exclusively populate single states in the first excited band we seek to coherently populate the charge localized state using a combination of three tailored pulses. As previously noted, the state $|\text{ion}, +\rangle$ can be reached via an intermediate transition through the second energy band. The state given by Eq. (8) is thus created by applying the first pulse to transfer 50% of the ground state to the second excited state. The second pulse further transfers the population in state $|e, -\rangle$ to the lowest ionic state $|\text{ion}, +\rangle$. The last pulse transfers the remaining 50% from the ground state to the upper ionic state $|\text{ion}, -\rangle$. In the upper panel of Fig. 4 we show the sequence of pulses applied to the system which initially is in the ground state. The pulses, labeled I, II, and III, have intensities $I_{\text{I}} = 0.39$ W/cm^2, $I_{\text{II}} = 0.39$ W/cm^2, and $I_{\text{III}} = 5.43$ W/cm^2 and durations $T_{\text{I}} = 127$ ps, $T_{\text{II}} = 225$ ps, and $T_{\text{III}} = 500$ ps. The frequencies are $\omega_{\text{I}} = 1.5$ THz, $\omega_{\text{II}} = 1.0$ THz, and $\omega_{\text{III}} = 2.5$ THz. The first and second pulses have envelope $f(t) = \sin^2(\frac{\pi}{T}t)$, whereas for the third pulse we have used a $\sin^2$ ramp-on of 10 cycles. At the end of the three pulses we have populated the charge localized state with 98% probability. We expect that this can be further increased by optimizing the pulse parameters.

In Fig. 4 we observe an interference between the states $|g, +\rangle$ and $|e, -\rangle$ during transition II and even larger oscillations between the $|\text{ion}, \pm\rangle$ states in III. The interference envelopes (beats) in, for instance, the nonresonant transition between the strongly coupled $|\text{ion}, \pm\rangle$ states is due to the nonzero initial population of the state $|\text{ion}+\rangle$. The nonresonant transitions in II and III are transient during the pulse(s) and do not affect the final state proba-

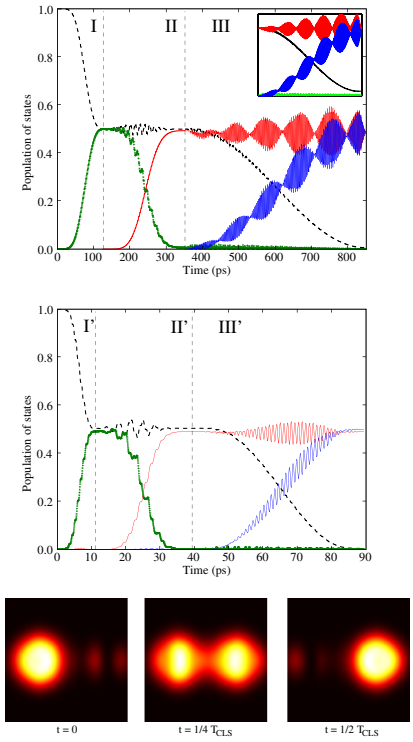

FIG. 4 (color online). Population of states during the sequence of pulses. The duration of the individual pulses is indicated by dashed vertical lines. The thin dashed line is the ground state population. The thick dotted line is the population of the excited state $|e, -\rangle$. The two lines that exhibit beats during pulse III are the population of the states $|\text{ion}, +\rangle$ (upper) and $|\text{ion}, -\rangle$ (lower). Upper panel: $\hbar\omega = 1$ meV and $d = 130$ nm. The inset shows the last transition modeled by a four-level system. Middle panel: $\hbar\omega = 3$ meV and $d = 60$ nm. Lower panel: Single-particle probability density for the field free propagation of the charge localized state at $t = 0$, $t = 1/4T_{\text{CLS}}$ and $t = 1/2T_{\text{CLS}}$. The period is $T_{\text{CLS}} = 180$ ps.

bilities. The dynamics during the third pulse (III) is fairly accurately modeled using only the four states, $|g, +\rangle$, $|e, -\rangle$, and $|\text{ion}, \pm\rangle$, as shown in the inset panel of Fig. 4.

In the middle panel we show the above described procedure applied to a system with stronger confinement strength, $\hbar\omega = 3$ meV, and interdot separation $d = 60$ nm. The field parameters here are $I_{\text{I}} = 12$ W/cm^2, $I_{\text{II}} = 3$ W/cm^2, and $I_{\text{III}} = 7$ W/cm^2 and durations $T_{\text{I}} = 11$ ps, $T_{\text{II}} = 28$ ps, and $T_{\text{III}} = 50$ ps. For the latter system we are able to use field amplitudes of about one magnitude greater than in our original system and thus reach the desired charge localized state a factor of 10 faster. In the lower panel we display the one-electron density for one half-cycle oscillation of the charge localized state. As expected we see a charge interchange between the two dots with period 180 ps. The fact that the $|\text{ion}, \pm\rangle$ are not the exact asymptotic states can be seen from a remaining probability for the electrons being in opposite dots even at maximum localization. This is visible as two weak dots on the right (left) in the first and last frames.

In conclusion, we have demonstrated controlled state to state transition in the strong coupling regime based on an exact numerical solution of the two-electron Schrödinger equation. We have shown that monochromatic microwave pulses with simple envelopes can drive the system between selected initial and final states. Further improvements of fidelity and transition times were achieved by employing a simple optimal control technique, which indicates that more general control schemes can improve the transition times even further. An oscillating charge localized state was produced using a robust three-step scheme to populate the two lowest entangled ionic states. Such charge oscillations can, in principle, be experimentally detected in quantum point contact devices and provide experimental information on the electronic structure of the double dot system [24,25]. The ability to control and detect the electronic properties is not only of fundamental interest, but is a prerequisite for effective optically based quantum information systems.

This research has been supported by the Research Council of Norway (RCN). The authors would like to thank Morten Førre for useful discussions.

[1] E. A. Stinaff *et al.*, Science **311**, 636 (2006).
[2] E. Cota, R. Aguado, and G. Platero, Phys. Rev. Lett. **94**, 107202 (2005).
[3] T. Hayashi *et al.*, Phys. Rev. Lett. **91**, 226804 (2003).
[4] J. R. Petta *et al.*, Phys. Rev. Lett. **93**, 186802 (2004).
[5] J. Zhang *et al.*, Phys. Rev. Lett. **97**, 226807 (2006).
[6] F. H. L. Koppens *et al.*, Nature (London) **442**, 766 (2006).
[7] D. Loss and D. P. DiVincenzo, Phys. Rev. A **57**, 120 (1998).
[8] X. Li *et al.*, Science **301**, 809 (2003).
[9] T. Meunier *et al.*, Phys. Rev. Lett. **98**, 126601 (2007).
[10] G. Platero and R. Aguado, Phys. Rep. **395**, 1 (2004).
[11] A. F. Terzis, S. G. Kosionis, and E. Paspalakis, J. Phys. B **40**, S331 (2007).
[12] G. M. Nikolopoulos, D. Petrosyan, and P. Lambropoulos, J. Phys. Condens. Matter **16**, 4991 (2004).
[13] A. Harju, S. Siljamäki, and R. M. Nieminen, Phys. Rev. Lett. **88**, 226804 (2002).
[14] A. Wensauer *et al.*, Phys. Rev. B **62**, 2605 (2000).
[15] V. Popsueva *et al.*, Phys. Rev. B **76**, 035303 (2007).
[16] P. S. Drouvelis, P. Schmelcher, and F. D. Diakonos, Europhys. Lett. **64**, 232 (2003).
[17] S. Selstø and M. Førre, Phys. Rev. B **74**, 195327 (2006).
[18] V. F. Krotov, *Global Methods in Optimal Control Theory*, Monographs and Textbooks in Pure and Applied Mathematics Vol. 195 (Marcel Dekker, New York, 1996).
[19] S. E. Sklarz and D. J. Tannor, Phys. Rev. A **66**, 053619 (2002).
[20] E. Räsänen *et al.*, Phys. Rev. Lett. **98**, 157404 (2007).
[21] E. Räsänen *et al.*, arXiv:0707.0179vl.
[22] Y. Silberberg, Nature (London) **430**, 624 (2004).
[23] M. Førre, Phys. Rev. A **70**, 013406 (2004).
[24] J. M. Elzerman *et al.*, Phys. Rev. B **67**, 161308 (2003).
[25] D. Wallin *et al.*, Appl. Phys. Lett. **90**, 172112 (2007).